The effects of AB_2 (A=Zr,Hf,Ti) additions on the free-iron content in ingotswith the initial composition of $Nd_{2.2}Fe_{14}B_{1.1}$

Kirby, Ken; Shaaban, Azizah; Walton, Allan; Kennedy, David; Williams, Andy J.; Brooks, Oliver; Sheridan, Richard; Harris, Ivor

DOI:
10.1016/j.jmmm.2020.167098

Document Version
Peer reviewed version

Citation for published version (Harvard):
Kirby, K, Shaaban, A, Walton, A, Kennedy, D, Williams, AJ, Brooks, O, Sheridan, R & Harris, I 2020, 'The effects of AB_2 (A=Zr,Hf,Ti) additions on the free-iron content in ingotswith the initial composition of $Nd_{2.2}Fe_{14}B_{1.1}$', *Journal of Magnetism and Magnetic Materials*, vol. 513, 167098. https://doi.org/10.1016/j.jmmm.2020.167098

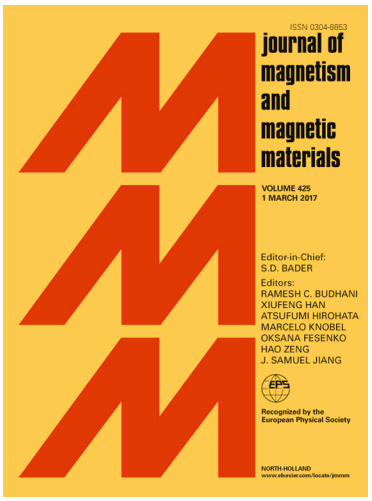

The effects of AB_2 (A=Zr,Hf,Ti) additions on the free-iron content in ingots with the initial composition of $Nd_{2.2}Fe_{14}B_{1.1}$

K. Kirby, A. Shaaban, A. Walton, D. Kennedy, A.J. Williams, O.P. Brooks, R.S. Sheridan, I.R. Harris

PII: S0304-8853(19)34036-3
DOI: https://doi.org/10.1016/j.jmmm.2020.167098
Reference: MAGMA 167098

To appear in: *Journal of Magnetism and Magnetic Materials*

Received Date: 29 November 2019
Revised Date: 10 April 2020
Accepted Date: 31 May 2020

Please cite this article as: K. Kirby, A. Shaaban, A. Walton, D. Kennedy, A.J. Williams, O.P. Brooks, R.S. Sheridan, I.R. Harris, The effects of AB_2 (A=Zr,Hf,Ti) additions on the free-iron content in ingots with the initial composition of $Nd_{2.2}Fe_{14}B_{1.1}$, *Journal of Magnetism and Magnetic Materials* (2020), doi: https://doi.org/10.1016/j.jmmm.2020.167098

The effects of AB_2 (A=Zr,Hf,Ti) additions on the free-iron content in ingots with the initial composition of $Nd_{2.2}Fe_{14}B_{1.1}$

K. Kirby[+], A. Shaaban*, A. Walton*, D. Kennedy*, A.J. Williams*, O.P.Brooks*, R.S. Sheridan* and I.R. Harris*.
+ Brookes Bell UK, Martins Building, Water Street, Liverpool, L2 3SX.
*School of Metallurgy and Materials, University of Birmingham, Edgbaston, Birmingham, B15 2TT, United Kingdom
Corresponding Author: Oliver Brooks O.P.Brooks@bham.ac.uk

Highlights:

- A 1 mol% addition of ZrB_2 to $Nd_{2.2}Fe_{14}B_{1.1}$ reduced Fe content from 12.34% to <1%
- Zr additions to $Nd_{2.2}Fe_{14}B_{1.1}$ were not as effective in reducing Fe content
- Other diborides were also shown to be effective in reducing the Fe content
- The addition of ZrB_2 to $Nd_2Fe_{14}B$ creates a deep eutectic in the phase diagram

Abstract:

Additions of zirconium diboride (ZrB_2), to small scale (~1 g) arc-melted (AM) and larger scale (5kg) book mould (BM) cast alloy with the composition $Nd_{2.2}Fe_{14}B_{1.1}$ (near to stoichiometric $Nd_2Fe_{14}B$) have been shown to be a very effective means of eliminating the free-iron content, which is present as a result of the peritectic nature of the $Nd_2Fe_{14}B$ phase. The effect of zirconium diboride in reducing free-iron content has been determined (1) magnetically by means of the Honda-Owen plots on the BM alloys and (2) by image analysis using scanning electron microscopy for both AM and BM alloys. Generally, for the BM alloys, both sets of measurements exhibited good agreement with a progressive reduction in the free-iron content with increasing additions of ZrB_2. Without any subsequent homogenisation treatment, zero free-iron was achieved in the AM and BM cast condition, after an addition of just 1 mole% of ZrB_2. Closely similar behaviour was observed with up to 1 mole% additions of the other Group 4 diborides, TiB_2 and HfB_2. High resolution scanning electron microscopy indicated that the diborides were embedded largely within the areas of Nd-rich material.

Key Words: metals and alloys; permanent magnets; rare earth alloys and compounds; mechanical alloying; microstructure; phase diagrams.

1. Introduction:

This investigation examined the possible effect of certain additions on the microstructure of $Nd_2Fe_{14}B$-type alloys to determine whether, with relatively small amounts of these additions, it is possible to reduce or even remove the presence of free-iron in the as-cast state of near stoichiometric compositions of $Nd_2Fe_{14}B$ (i.e. around the composition $Nd_{11.765}Fe_{82.353}B_{5.882}$). It is well known [1, 2] that the $Nd_2Fe_{14}B$ phase forms by means of a peritectic reaction with iron and a Nd-rich liquid phase. This often results in an incomplete reaction such that book mould cast (BM)-type alloys close to stoichiometry contain a significant proportion of free-iron and hence the alloy requires a prolonged homogenisation process in order to remove the free-iron dendrites [3]. This adds appreciably to the time, energy and hence cost required to produce magnets based on the near-stoichiometric compositions.

A current solution to this involves the employment of off-stoichiometric compositions such as Neomax-type alloys (~$Nd_{15}Fe_{77}B_8$) where the form of the phase diagram allows the peritectic reaction to be avoided in this (or close to this) Nd and B rich composition [4,5]. Thus, avoiding the free-iron phase in the BM condition, which lowers the coercivity of NdFeB-type magnets, and producing an alloy with a majority $Nd_2Fe_{14}B$ phase, and minority Nd-rich and $NdFe_4B_4$ phases.

The draw back with this approach is that the requirement for even larger values of $(BH)_{max}$, closer to the theoretical upper limit of 640 kJ/m^3, means that fully dense, anisotropic magnets are required with ever closer compositions to that of stoichiometric 2:14:1. This is often accomplished by rapid casting methods such as strip casting (cooling rate of ~10^3 K/s) [6] or even more rapid cooling rates with melt spinning (~10^6 K/s) [7], producing flakes of material which must be subsequently processed as a powder. In the latter case, unless upset-forging [8] is applied then only isotropic magnets can be produced.

Very recent work [6, 7] has demonstrated the application of the HyDP (Hydrogen Ductilisation Process) whereby normally hard and brittle alloys based on $Nd_2Fe_{14}B$ can, in the solid hydrogen disproportionated state, become extremely ductile even at room temperature, and subsequently can be restored to the hard ferromagnetic state by the desorption of the hydrogen. This could allow for production/shaping of magnets from book mould material without the need for powder processing. However, when HyDP is applied to the Neomax-type alloys, then excessive cracking of the $NdFe_4B_4$ phase is observed during deformation and to avoid this problem, a long (>18 hour) disproportionation of the $NdFe_4B_4$ phase is required [10,11].

All of these problems point to the need to produce a single phase $Nd_2Fe_{14}B$-type composition close to that of stoichiometry but in the book mould cast condition (possibly after a short homogenisation treatment). Thus, allowing HyDP to produce a fully dense magnet from book mould material, with a maximum amount of hard magnetic phase and reduced fracturing during the processing.

The present paper reports the outcomes of an investigation into the effects of additions of ZrB_2 on the BM-type alloys close to the $Nd_2Fe_{14}B$ composition and the reduction of free-iron in the microstructures. As a precursor to the study of the BM material, the effect of these additions on the homogeneity of small (~1 g) arc-cast samples have been studied. The employment of this particular method of producing the alloys offers the following advantages:

1. The very high melting temperature used in AM casting means that high melting point additions (such as ZrB_2) can be added directly to the $Nd_2Fe_{14}B$ material, whereas in the subsequent BM casting techniques (at Less Common Metals Ltd., LCM) the ZrB_2 additions could only be made when incorporated in the overall compositions, increasing the boron content using ferro-boron and the Zr addition as metallic sponge. The compositions of these alloys are shown in Table 1.
2. In the AM melting process there is a very large temperature gradient from the top to the bottom of the sample (~1 g) such that, next to the water-cooled copper hearth, very rapid solidification occurs due to very high cooling rates. This should be close to those employed in the melt-cast condition and hence the effectiveness of this treatment could be indicated from the microstructure within this zone.

3. The microstructure of the complete AM sample can be studied from this zone (next to the hearth) to the top of the NdFeB button and should provide valuable evidence as to the effectiveness of particular additives which can then be studied on a larger scale (~5 kg) using the induction-based BM casting method.

Table 1. BM casting compositions for $Nd_{2.1}Fe_{14}B_{1.1}$ and with 1 mole% ZrB_2

Element	Atomic Ratio	At%
Nd	2.2	12.72
Fe	14	80.92
B	1.1	6.36
		+1% ZrB2
Nd	2.2	12.72
Fe	14	80.92
B	1.1	8.36
Zr		1

ZrB_2 and other Group IV diborides (TiB_2 and HfB_2) are well established grain refining additions[12]. The phase diagram for the B-Zr system is shown in Figure 1 [8, 9].

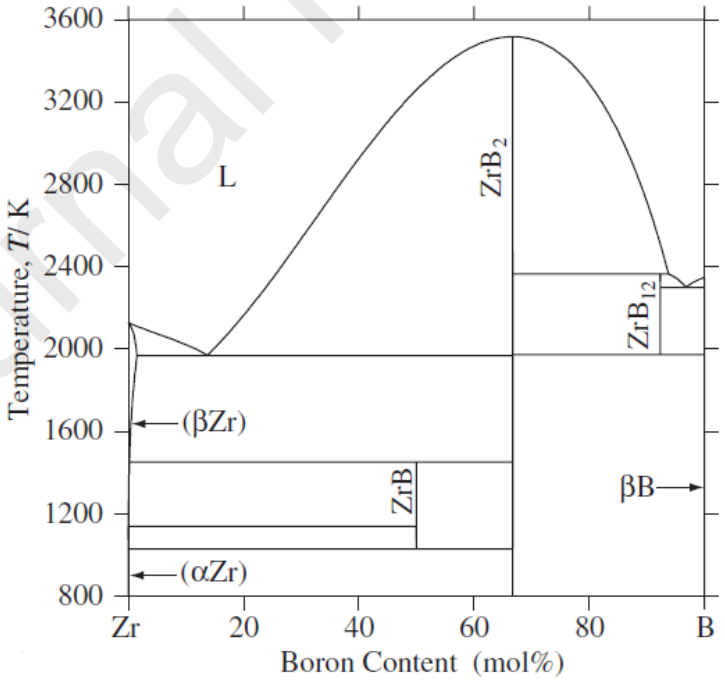

Figure 1. B-Zr Phase diagram [8, 9]

It can be seen clearly from this diagram that ZrB_2 is an extremely stable congruent phase with a melting point of 3518 K (3245 ºC). It can also be seen that there is little solubility of B

in Zr, forming a eutectic close to 86% Zr (namely 14% B) and ZrB_2 would, therefore, be expected to form a eutectic with the much less stable, and peritectic, $Nd_2Fe_{14}B$ phase close to this composition. In general, the form of the phase diagram with $Nd_2Fe_{14}B$ would be expected to have the general appearance shown in Figure 2, with a deep eutectic at with increased ZrB_2. The actual phase diagram will be a little more complicated because, the compositions employed in the present work ($Nd_{2.2}Fe_{14}B_{1.1}$) is on the Nd-rich side of stoichiometry.

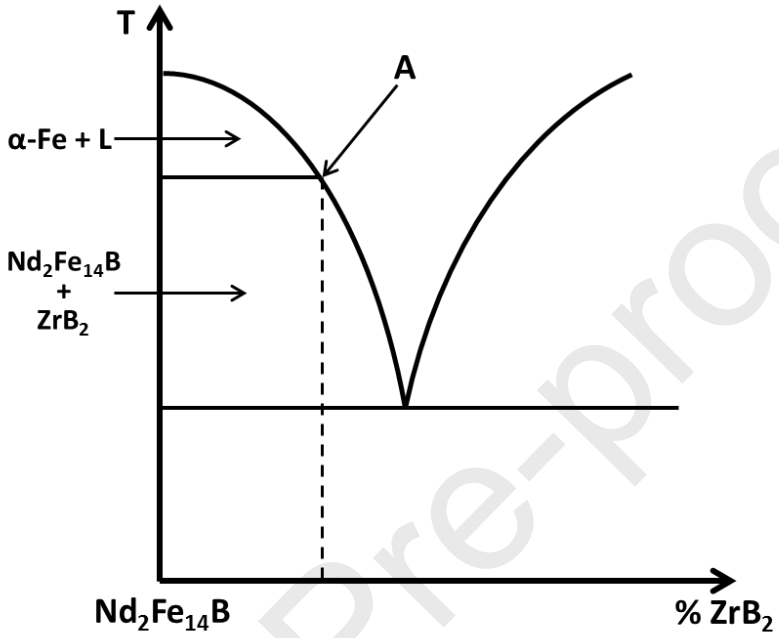

Figure 2. Schematic of the hypothetical phase diagram for the NdFeB system with ZrB_2 additions, created by the authors

In the present work the eutectic mixture would be expected to consist of a combination of ZrB_2 (minority phase), Nd-rich phase and $Nd_2Fe_{14}B$. A critical point in this diagram is labelled 'A', where the peritectic isotherm meets the Fe-liquidus so that, compositions at or in excess of A could be cast without crossing the peritectic isotherm and therefore expect to consist of a matrix of $Nd_2Fe_{14}B$ and a grain boundary eutectic of $Nd_2Fe_{14}B$ + Nd-rich + ZrB_2. As there is a slight excess of Nd-rich material then this would be a component of the grain boundary phase. Similar arguments could also be expected to apply to additions of TiB_2 and HfB_2, where similar, very stable diboride phases exist [15,16].

The overall compositions studied in this work can be represented by the general formula:

$$(Nd_{0.127}Fe_{0.809}B_{0.063})_{100-3x}(AB_2)_x \quad \text{at\%}$$

Where A could be Hf, Ti or Zr. These alloys covered the range from 0-2 mole% ZrB_2. An alternative representation is $Nd_{2.1}Fe_{14}B$ which indicates clearly the slight Nd-rich nature of the alloys.

Work on the BM alloys extended into additions of Zr alone to observe effects on free-iron content of the Zr as it combines with the B content over and above that needed to form the $Nd_2Fe_{14}B$ phase. Previous works [17] have shown that the addition of Zr reduce the free-iron

dendrites and that platelet-like precipitates formed in the grain boundary phase which were believed to be ZrB_2. The atomic percentage of B in $Nd_2Fe_{14}B$ is 5.88 at% whereas in $Nd_{2.2}Fe_{14}B_{1.1,}$ B it is 6.36 at%.

Experimental Methods:

The arc cast samples were produced by loading the alloy constituents (Nd, Fe, Fe_2B, ZrB_2) onto a copper hearth in an arc melting furnace along with an oxygen getter button. The system was then evacuated and argon flushed 5 times to remove oxygen before finally evacuating to rotary pump vacuum (10^{-2} mbar). The getter button was melted first, at a sufficient distance from the sample to avoid any interaction, to react with any remaining oxygen before arc melting the constituents into a molten pool, cooling and re-melting 4 times to ensure efficient mixing of the constituents before rapid cooling on the water-cooled copper hearth.

For the BM samples ZrB_2 could not be directly melted in, therefore, the experimental alloys were created using a mixture of ferro-boron, zirconium, neodymium and iron to create the alloy $Nd_{2.2}Fe_{14}B_{1.1}$ + ZrB_2, to mimic the compositions used for the AM samples. This ensured dissolution of the elements in controlled and limited temperatures, whereas, additions of ZrB_2 were possible with the AM castings due to high energy intensity from the arc melt ensuring dissolution of the diboride.

The BM ingots (~5 kg) have been produced at Less Common Metals Ltd, Ellesmere Port UK. according to standard procedures and consist of the $Nd_{2.2}Fe_{14}B_{1.1}$ composition together with increasing additions of ZrB_2 in increments of 0.2 mole% up to 1.0 mole % and then a jump to 2 mole %. These compositions are shown in Table 2.

Table 2. Composition of alloys used in this study (at%), measured by ICP-OES.

Alloy	Nd	Fe	B	Zr
0 mole % ZrB_2	12.72	80.92	6.36	0.00
0.2 mole % ZrB_2	12.65	80.43	6.72	0.20
0.4 mole % ZrB_2	12.57	79.94	7.09	0.40
0.6 mole % ZrB_2	12.50	79.45	7.45	0.60
0.8 mole % ZrB_2	12.42	78.98	7.82	0.80
1.0 mole % ZrB_2	12.35	78.47	8.18	1.00
2.0 mole % ZrB_2	11.98	76.02	10.00	2.00

In the present investigation the free-iron content in the BM alloys produced at LCM has been determined magnetically by means of the Honda-Owen (H-O) method. A sample of 50-70 mg was taken from the centre of each ingot and mounted in the LakeShore 7000 vibrating sample magnetometer (VSM). Measurements of the magnetisation vs applied field at room temperature and at 400 °C were made and the data at 400°C was used to determine a series of H-O plots from which the free-iron content could be determined. Because, at room temperature, the alloys contain two ferromagnetic components, the H-O measurements require heating a particular sample to 400 °C (above the Curie point of $Nd_2Fe_{14}B$) in the VSM and then determining the magnetic susceptibility (χ=M/H) as a function of 1/H. the free-iron content can then be determined by the following equation:

$$X_{mag} = \frac{Fe \times M_{s(Fe)}}{H} + X_{para}$$

Providing the ferromagnetic impurity (in this case free-iron (Fe)) is fully saturated ($M_{s(Fe)}$) then there will be a linear relationship for the above equation, whereby the slope is determined by the amount of free-iron and the extrapolated value of the susceptibility (X_{mag}) at infinite field is predominantly, the paramagnetic susceptibility (X_{para}) of the $Nd_2Fe_{14}B$ matrix at 400 °C. The metallographic studies indicate that there will also be a small magnetic contribution from the ZrB_2 phase but this should not affect the calculated iron content.

Independently, the free-iron content can also be determined more directly by means of the image analysis of the scanning electron microscope (SEM) metallographic images of the AM and BM samples. The area fractions of free-iron were determined using image analysis software (ImageJ) of several of the SEM images and the data was then compared with that determined from the H-O studies. For microscopy, the alloys were sliced using a diamond saw and mounted in conductive Bakelite, before being ground with P120, P240, P480, P800 and P1200 SiC grinding paper, before being polished with 6 µm, 1 µm, 0.25 µm diamond compounds.

Samples of the BM alloys were sectioned and ground to a flat finish for XRD studies to compare the variation of the lattice spacings of the tetragonal $Nd_2Fe_{14}B$ matrix phase with increasing additions of ZrB_2

2. Results and Discussion:

3.1 Arc-Melted Alloys:

The microstructure of the ZrB_2-added arc-melted NdFeB-alloy buttons are shown for various cross sections in Figure 3, which consisted of 1 g total weight with thicknesses between 3.5-4.5 mm. A columnar texture (region Q) can be observed at the cut surface along the cooling direction, perpendicular to the copper hearth (in these images the copper hearth is at the bottom of the cross-section). Furthermore, two distinct regions with free-iron can be observed at the top (region P) and bottom (region R at the cooled copper hearth) of the microstructures. As a typical example, the effects of ZrB_2 addition of 0.2, 0.4 and 0.6 mole% are shown in Figure 4 at higher magnification for the lower sections of the buttons.

It can be seen that with increasing ZrB_2 addition, there is a very significant reduction in the free-iron content. Near the cooled edge, the region R reduces in size and moves away from the edge of the sample with increased additions, creating an iron-free zone. In the 0.8 mole% ZrB_2 sample free-iron is confined to the top layer of the arc melted sample and the 1 mole% sample indicates the complete disappearance of the free-iron. The dark areas observed in the 1 mole% sample can be ascribed to porosity in the sample caused by the arc-melting process. For the lower percentage additions, the dark areas in Figure 3 are ascribed to large areas of Nd-rich within the microstructures.

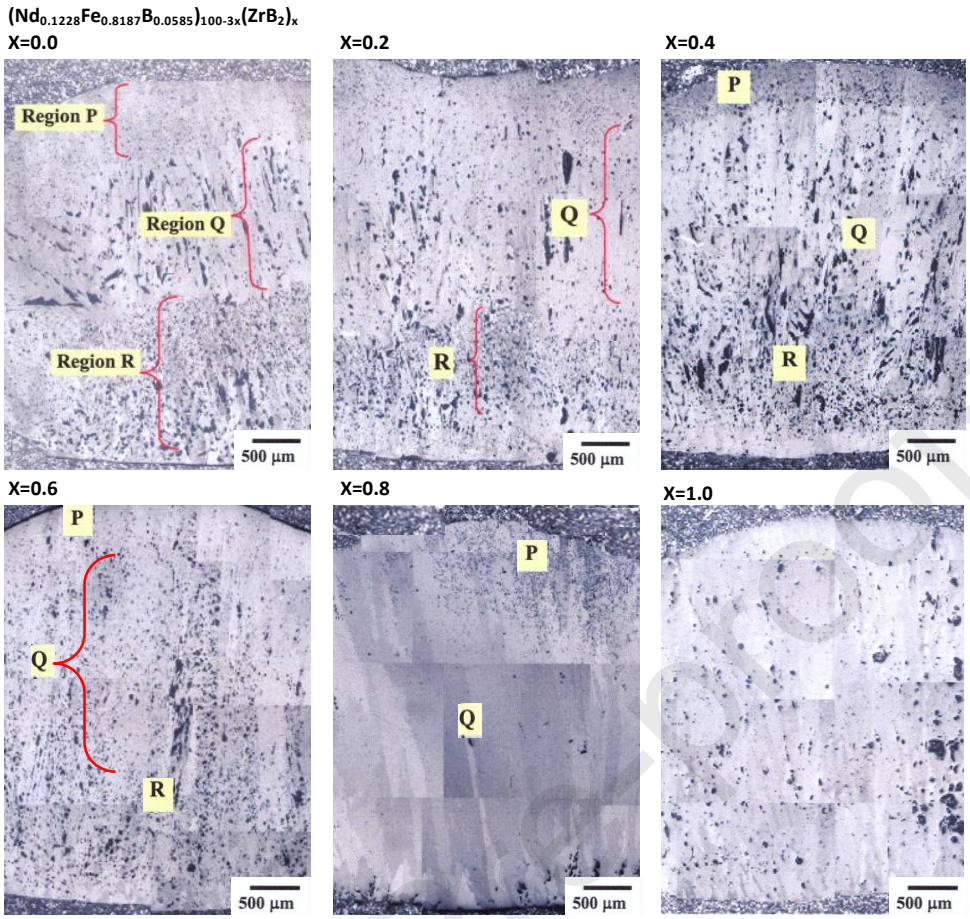

Figure 3. Optical micrographs showing composite cross sections of arc melted NdFeB alloys containing (top to bottom) 0.0 to 1.0 mole% ZrB_2. Region P contains Fe dendrites in the upper section, Region Q shows the columnar $Nd_2Fe_{14}B$ structure and Region R is rich in free-iron in the lower section.

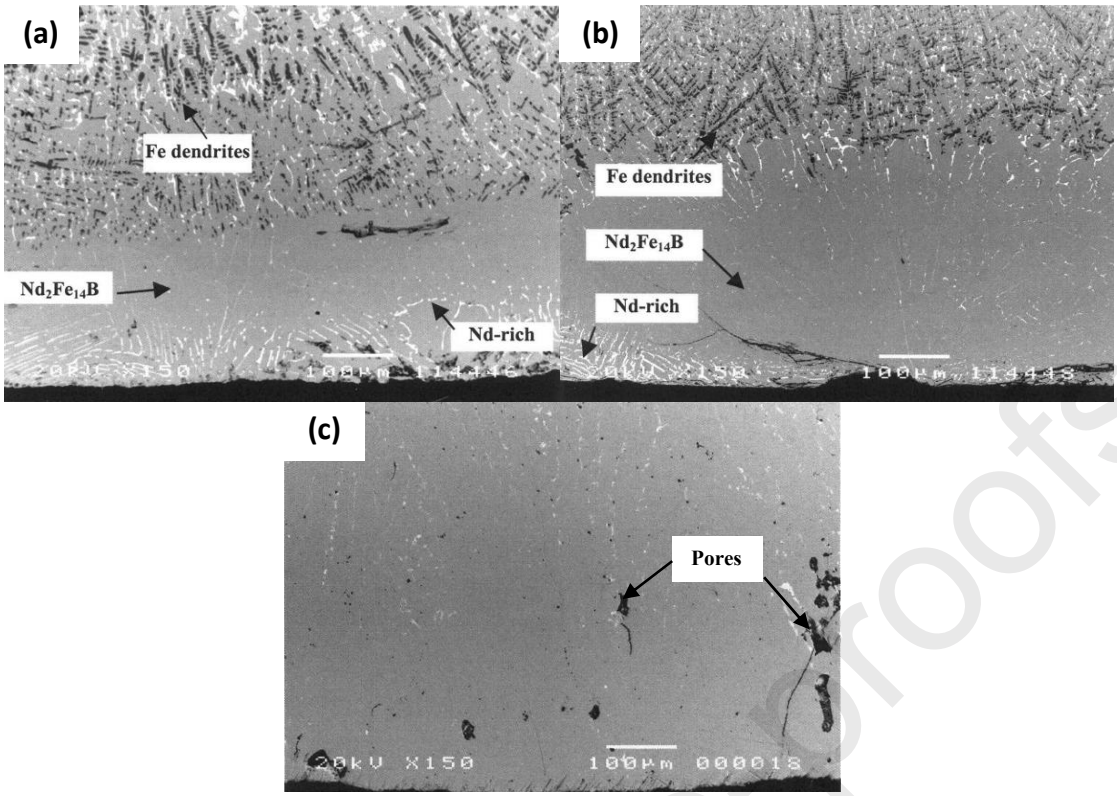

Figure 4. Back-scattered SEM micrographs showing microstructures of arc melted NdFeB alloys containing (a) 0.0 mole%, (b) 0.6 mole% and (c) 1.0 mole% ZrB_2

The quantitative analysis of the iron-free zones is shown in Figure 5. The thickness of the region which has none or reduced free-iron (close to the copper hearth) can be expressed as the ratio:

$$d / h (\%)$$

Where d=length of the iron-free zones and h=total height of the sample. Thus 100% represents complete removal of the free-iron dendrites. Analysis of several images of the cross-sections of each sample were used to calculate this ratio. In figure 5 it can be seen that the ZrB_2 additions in excess of 0.4 mole% are particularly effective and achieve 100% removal of free-iron at the addition of 1 mole% ZrB_2. This sharp upturn in effectiveness could indicate the interception of the peritectic isotherm with the liquidus, which could occur between 0.4 and 0.5 mole% ZrB_2.

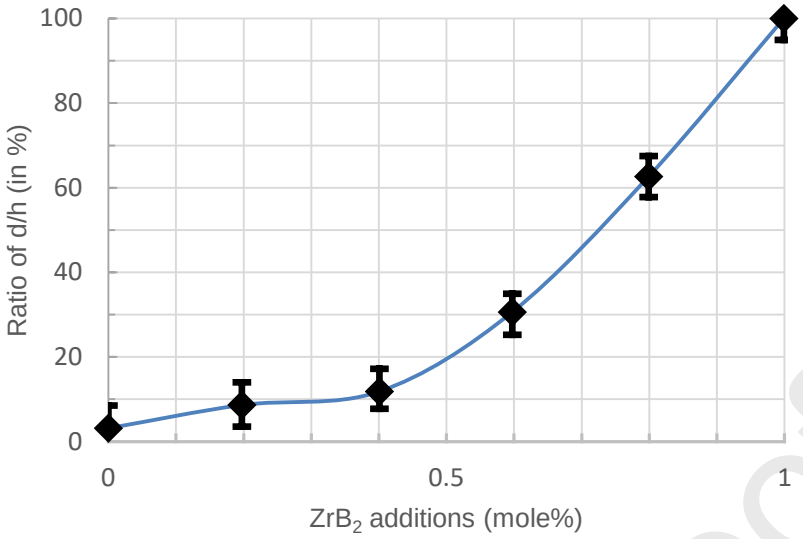

Figure 5. Estimated iron-free region of each ingot (expressed as a ratio) with increasing ZrB_2 addition.

The arc melted samples indicated clearly that, under these conditions, 1 mole% addition of ZrB_2 was required to remove all of the free-iron content without the need for a subsequent homogenisation treatment. The next stage was to look at the effect of operating on a possible industrial scale by examining the effect of ZrB_2 additions on the free-iron content in book mould cast (BM-type) industrial alloys. Because of the exceptionally high melting point of the ZrB_2 addition (3245 ºC) combined with its low density, the ZrB_2 powder could not be induction melted coherently as in the arc-melter. In the case of the BM alloys which often have a weight >5 kg, it was necessary to produce a similar alloy range by adding Zr metal and B in the form of ferro-boron as described in Table 1.

3.2 BM Alloys: Honda-Owen (H-O) Measurements:

A typical set of magnetisation plots for the 1.0 mole% ZrB_2 alloy are shown in Figure 6 with the corresponding H-O plot. The latter exhibits excellent linearity and yields a free-iron content of 0.84±0.26%.

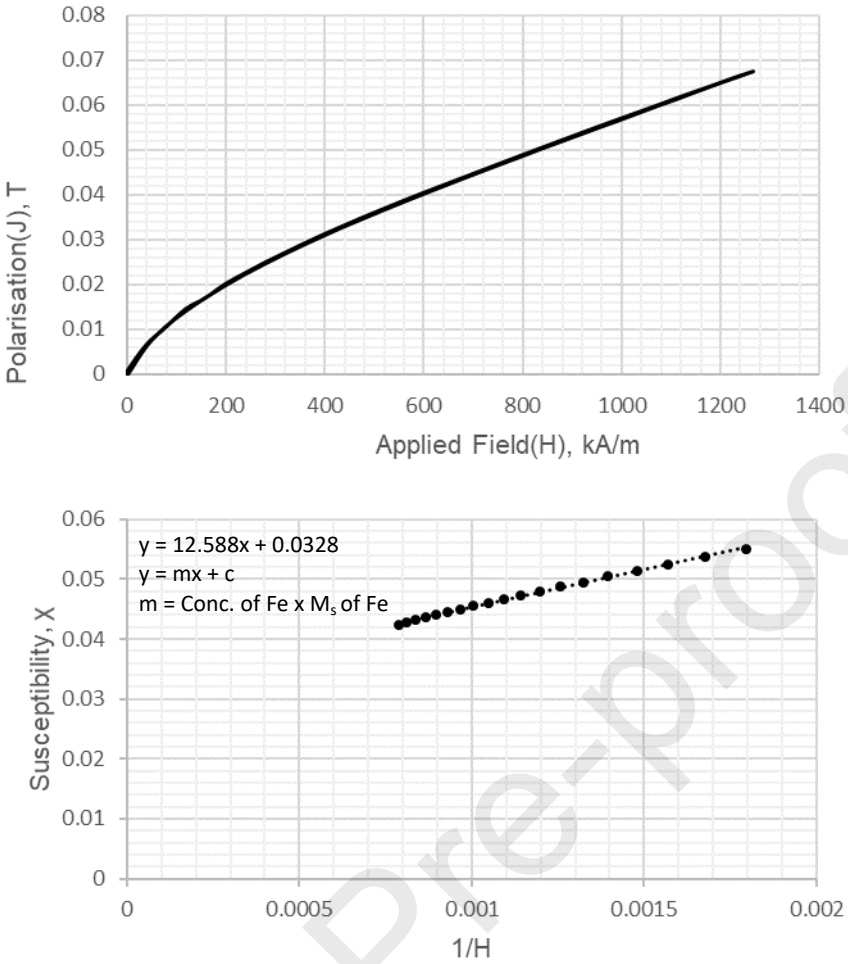

Figure 6. Magnetisation plots for BM alloy + 1 mole% ZrB_2 at 400 °C (top) and the Honda-Owen plot (bottom)

All the H-O measurements are summarised as a function of mole% ZrB_2 in Figure 7 and this indicates almost complete removal of the free-iron at 1 mole% ZrB_2. This remains the same for the addition of 2 mole% ZrB_2.

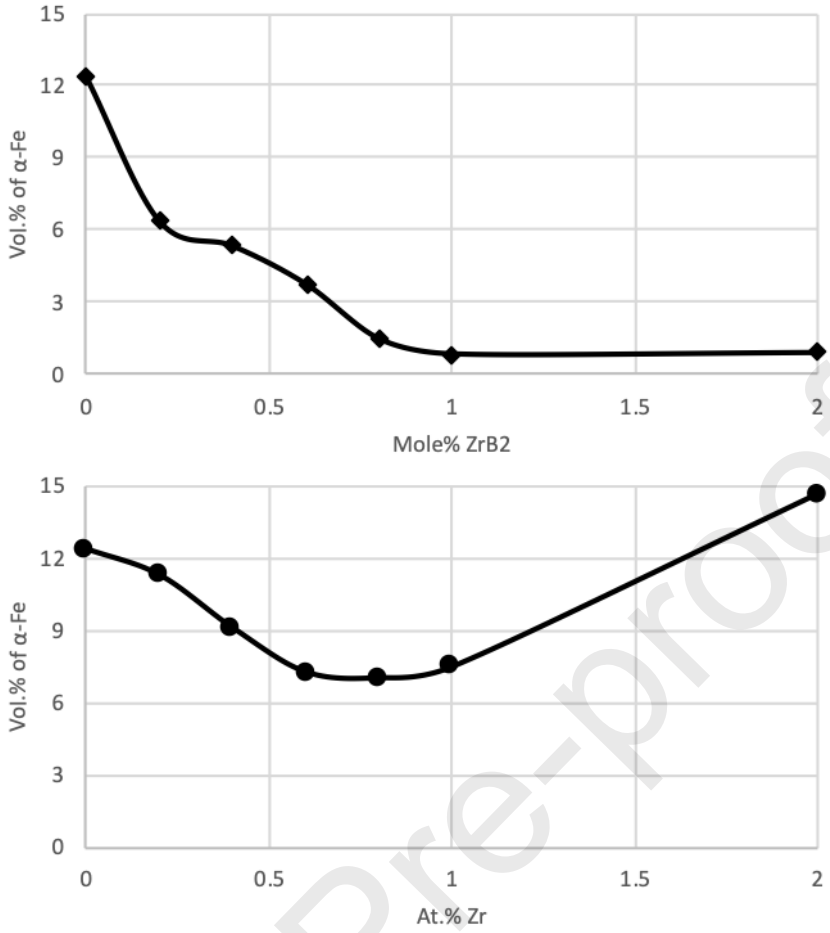

Figure 7. Free-iron content as a function of ZrB_2 (top) and Zr (bottom) additions, as measured by the Honda-Owen method

A similar set of measurements have been carried out with additions of zirconium metal, not the diboride, and the data from a similar set of H-O measurements is shown in Figure 7. This variation is distinctly different to that shown previously and the persistence of the free-iron can be understood in terms of the zirconium additions combining with the boron in the $Nd_{2.2}Fe_{14}B_{1.1}$ to form the stable ZrB_2 phase during casting. With low additions of Zr this phase can freely form and produce a similar effect to the ZrB_2 additions. However, with larger additions of Zr metal the formation at the ZrB_2 phase will possibly deplete the $Nd_2Fe_{14}B$ phase of boron, resulting in the formation of some Nd_2Fe_{17} phase or free-iron within the surrounding microstructure [18], hence the increase in vol% of iron in figure 7. Further study is required to confirm this behaviour.

3.3 Metallographic Studies:

In addition to the magnetic investigations described earlier, the present series of BM alloys have also been characterised by image analysis of the backscattered SEM images. On adding ZrB_2, the changes observed in the microstructure of the BM alloys are summarised in Figure 8 and the main features of all these microstructures are the black areas of free-iron dendrites, the grey areas of the $Nd_2Fe_{14}B$ phase and the white regions of the Nd-rich phase which, on close examination, is shown to contain needles of ZrB_2 (Figure 9). The morphology of the free-iron and Nd-rich phases within these microstructures is significantly different to

that observed in the AM material, this is due to the much slower rate of cooling in the BM process. There are also several dark areas in Figure 8 (f&g) which are associated with porosity in the sample and not free-iron as with the previous micrographs.

The predominant feature of all these micrographs (as with the studies of the AM samples) is the progressive diminution in the areas of free-iron dendrites with increasing additions of ZrB_2 such that, at 1 mole%, there is little or no free-iron present in the samples. This situation persists for the addition of 2 mole% (Figure 8g) and the Nd-rich and ZrB_2 (white areas) appears to exist as a component of a eutectic mixture at the grain boundaries. This is more evident in the microstructure of the 1 mole% ZrB_2 alloy (Figure 9a) which has been heat treated at 900 °C for 2 hours. The possibility of a eutectic type reaction will be discussed later. Closer examination at higher magnification of the Nd-rich areas indicates clearly the embedded presence of needles which can safely be assumed to be based on ZrB_2 (Figure 9b).

The results of the phase fraction image analysis of the SEM microstructures shown in Figure 8 are summarised in Table 3 and Figure 10. This variation is in good agreement with the H-O results shown in Figure 7 and both show the importance of the 1 mole% ZrB_2 composition. The largest disparity in the two variations occurs at zero mole% ZrB_2 where the H-O results appear to indicate a higher free-iron content. Some of these discrepancies can be attributed, in part at least, to the residual iron indicated by the H-O measurements at 1 and 2 mole% ZrB_2 which could be due to some limited oxidation of the samples. The free-iron content obtained by the two methods are summarised in.

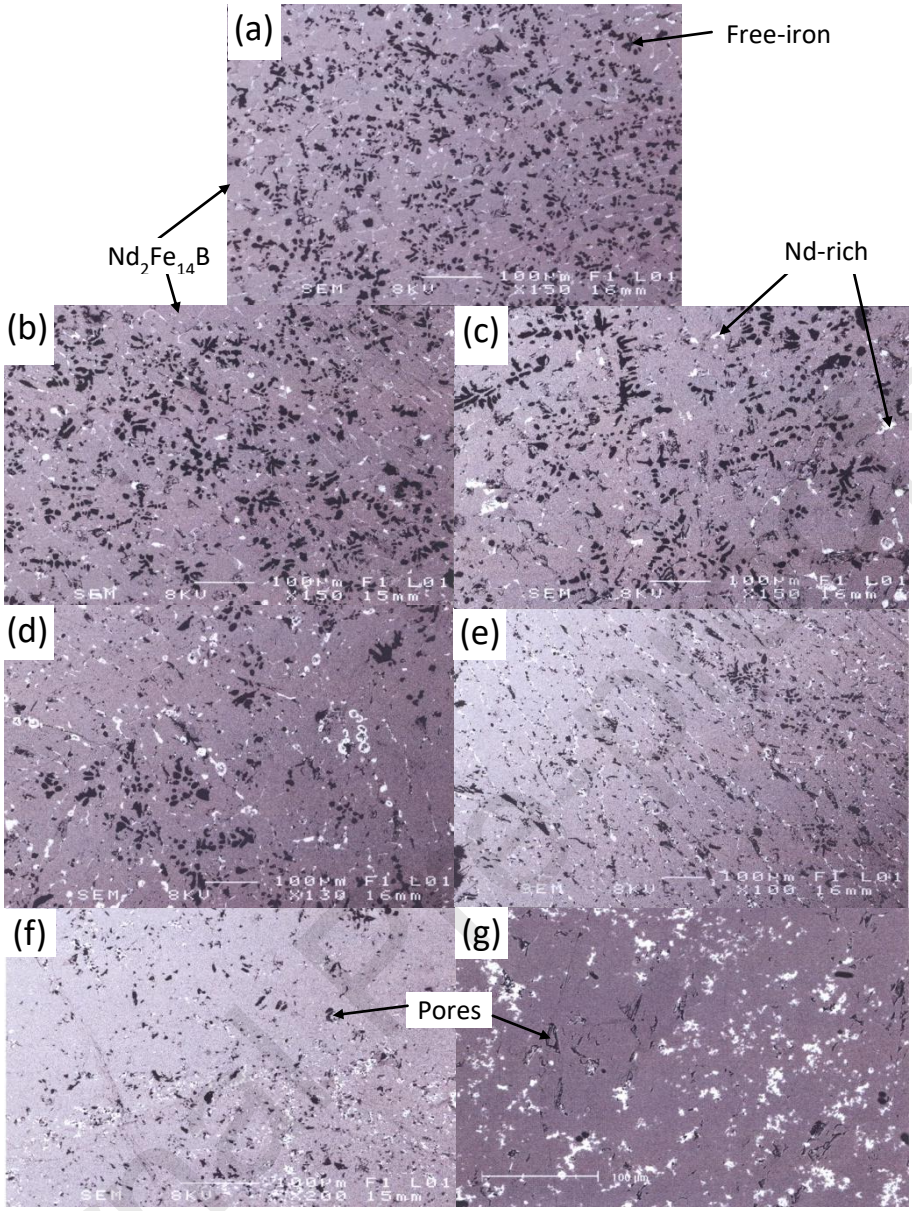

Figure 8. Backscattered SEM images of BM alloys containing various ZrB_2 contents in mole%: a) 0%, b) 0.2%, c) 0.4%, d) 0.6%, e) 0.8%, f) 1.0%, g) 2.0%.

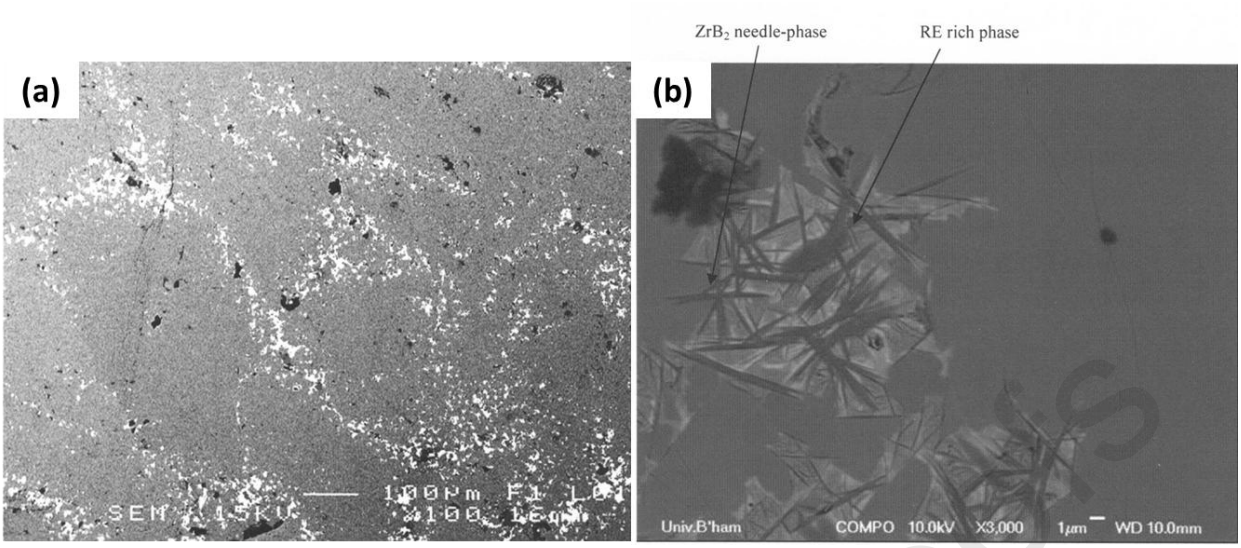

Figure 9. Backscattered SEM image of BM alloy (a)+1.0 mole% ZrB_2 heat treated at 900 °C for 2 hours and (b) showing ZrB_2 needles within the Nd-rich grain boundary phase.

Table 3. Free-iron content of BM alloys with additions of ZrB_2 analysed by H-O and image analysis

Mole% ZrB_2	Free-iron Content From H-O (±0.26%)	Free-iron from Image Analysis (±0.5%)
0	12.36	8.36
0.2	6.35	7.75
0.4	5.33	5.06
0.6	3.74	3.14
0.8	1.46	0.96
1.0	0.84	0
2.0	0.97	0

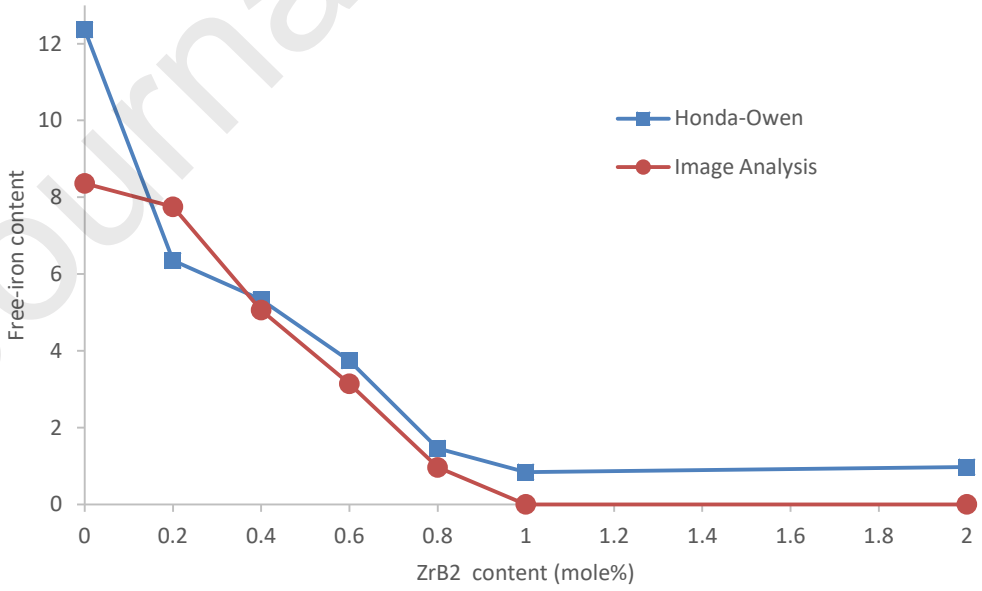

Figure 10. Variation of free-iron content as a function of ZrB_2 additions, measured by Honda-Owen and image analysis techniques

X-Ray Diffraction (XRD) Studies:

The lattice spacings of the tetragonal $Nd_2Fe_{14}B$ matrix phase with increasing additions of ZrB_2 are summarised in Table 4. Only minor changes have been observed in the a- and c-spacings, indicating little solubility range in this region of the $Nd_2Fe_{14}B$-ZrB_2 system. This is consistent with the reported stability of ZrB_2 and with the lack of any significant change in the Curie point of the $Nd_2Fe_{14}B$ phase from 0 to 1.0 mole% ZrB_2, as determined by differential scanning calorimetry (DSC) measurements (to be published).

Table 4: Variation of a-spacing and c-spacing as a function of ZrB_2 addition obtained from XRD Studies.

Alloy (mole% ZrB_2)	a-spacing (+/-0.001)Å	c-spacing (+/-0.001)Å
0	8.811	12.206
0.2	8.803	12.192
0.8	8.792	12.189
1.0	8.797	12.198
2.0	8.803	12.197

3.4 The Effects of Additions of Other Group 4 Diborides.

3.4.1 TiB_2 Additions:

In the present studies, the effects on the microstructure of BM alloys of adding 0.6 and 1.0 mole% of TiB_2 to $Nd_{2.2}Fe_{14}B_{1.1}$ have also been examined and very similar results to those observed for ZrB_2 additions have been obtained. These can be seen in the SEM, backscattered images shown in Figure 11. Figure 11a shows the BM alloy with 0.6 mole% TiB_2 and this has a similar appearance to the corresponding ZrB_2 alloy (Figure 8d)). The microstructure consists of dendrites of free-iron, a light contrast Nd-rich area at the grain boundaries with associated needles of TiB_2, and the grey $Nd_2Fe_{14}B$ matrix phase (confirmed by EDS). Higher magnification images of the grain boundary regions revealed clearly the needles of TiB_2 and these have also been observed (less clearly) in the ZrB_2-based alloys. The 1 mole% TiB_2 BM alloy is shown in Figure 11c, and has only a small content of free-iron dendrites (see Table 5).

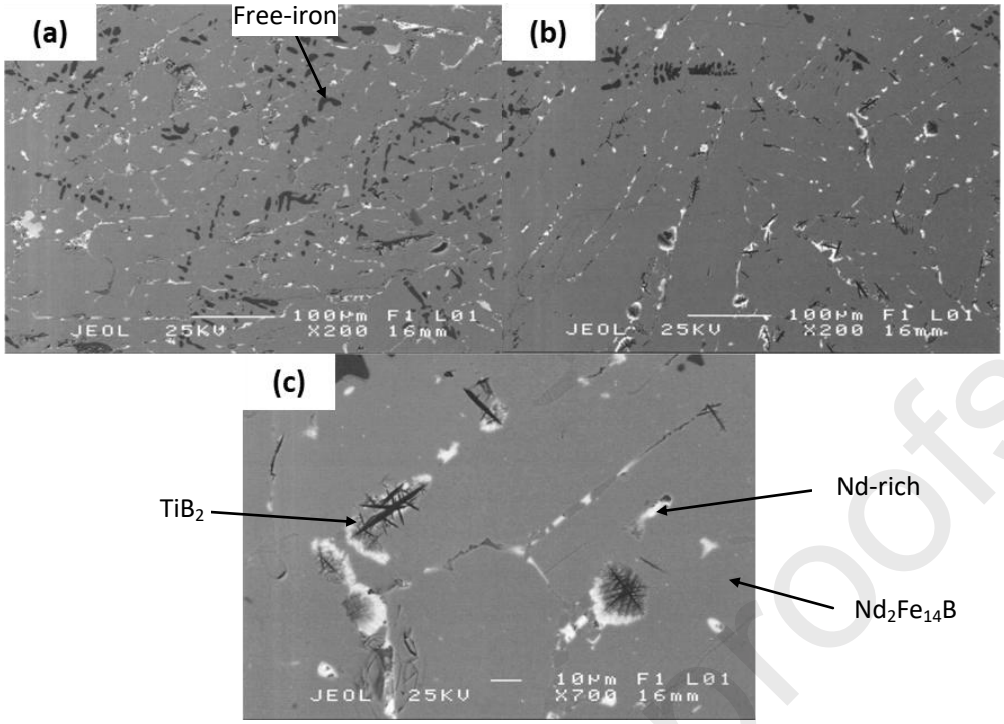

Figure 11. Backscattered SEM images of BM alloys containing (a) 0.6 mole% and (b) 1.0 mole% TiB_2. (c) Backscattered SEM images showing TiB_2 needles in a BM alloy containing 1 mole% TiB_2

3.4.2 HfB_2 Additions:

The effect of additions of HfB_2 are shown in Figure 12. Here a similar pattern of behaviour is observed, with the 1 mole% HfB_2 BM ingot exhibiting a complete absence of the free-iron and what appears to be a eutectic mixture at the grain boundaries. A higher magnification image of the grain boundary region (Figure 12c) shows the HfB_2 (A) which has formed from the melt with the preferential growth of the hexagonal faces giving rise to approximate six-fold symmetry. The results of the image analysis of the TiB_2 and HfB_2 series are summarised in Table 5 and this indicates that, in these cases, the HfB_2 additions are somewhat more effective than those of TiB_2.

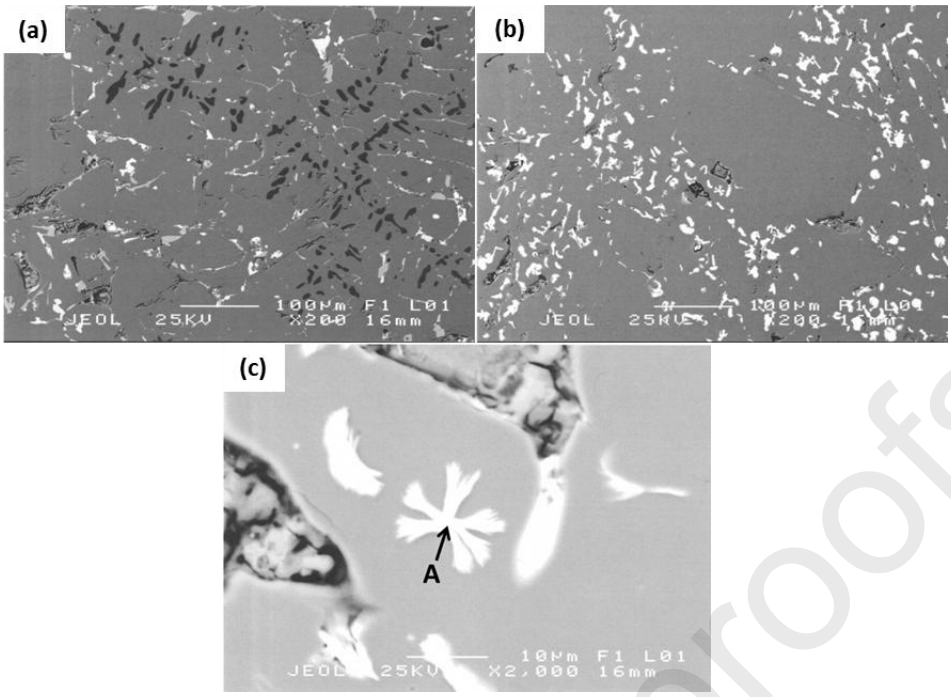

Figure 12. Backscattered SEM images showing BM alloys containing (a) 0.6 mole% and (b) 1.0 mole% HfB_2. (c) Backscattered SEM image showing the formation of HfB_2 (labelled A) in a BM alloy containing 1 mole% HfB_2.

Table 5. Image Analysis of the Free-iron Content for additions of TiB_2 and HfB_2.

Mole% addition	Free-iron Content with TiB_2 addition (± 0.5%)	Free-iron Content with HfB_2 addition (± 0.5%)
0	8.09	8.09
0.6	3.22	3.22
1.0	0.94	0

3.5 A Possible Explanation for the Role of the Diborides

In the present investigation, the most detailed examination has been carried out on the effect of ZrB_2 additions on the AM and BM microstructure of the near stoichiometric $Nd_2Fe_{14}B$ alloy ($Nd_{2.2}Fe_{14}B_{1.1}$). The common structure, great stability and very similar microstructures of the BM alloys indicate that there could be a general explanation and mechanism for the behaviour observed in all three systems (ZrB_2, TiB_2 and HfB_2), indeed the applicability could stretch to an even wider range of borides.

The observation of a possible ternary eutectic mixture close to the composition of $Nd_2Fe_{14}B$ and the reduction and eventual removal of the free-iron at 1 mole % AB_2 (where A=Ti, Zr or Hf) can be explained in terms of a eutectic reaction close to the $Nd_2Fe_{14}B$ composition between this phase and AB_2, along with the narrowing of the high temperature iron + liquid field and at the 1 mole% AB_2 composition, the peritectic isotherm could meet the liquidus. This is illustrated generally in Figure 2. If this explanation is correct, then these particular phase reactions will require precise DSC/DTA measurements which will be the subject of future investigations.

Having established the effectiveness of these additions the BM alloys will now be examined as a starting material for the production of permanent magnets based on various production techniques, and in particular the Hydrogen Ductilisation Process (HyDP) for cold working permanent magnet materials of the NdFeB type. By utilising a composition of NdFeB which produces a lower content of the brittle $NdFe_4B_4$ phase and introducing these di-boride additions to remove any free-iron, it may be possible to produce a book mould cast alloy that would be ideal for cold working during HyDP and that could also produce significant magnetic properties. However, studies are required on the influence of these di-boride phases on the hydrogen reaction kinetics, cold working behaviour and magnetic properties during HyDP.

3. Conclusions:

(1) The present results all agree with the alloy model presented at the beginning of this paper which stated that the additions of ZrB_2 to $Nd_2Fe_{14}B$ would create a deep eutectic in the phase diagram and that after a critical point (A) it would be possible to completely avoid the αFe + L peritectic isotherm and go directly to forming $Nd_2Fe_{14}B$ + Nd-rich + ZrB_2.

(2) The progressive effects of adding ZrB_2 to the composition $Nd_{2.2}Fe_{14}B_{1.1}$ was first established using the arc melting technique, showing that an iron-free zone formed close to the cooled Cu hearth and that this zone appears to visibly decrease in size with the addition of ZrB_2.

(3) The free-iron content in the $Nd_2Fe_{14}B$-ZrB_2 alloys was determined using the Honda-Owen (H-O) magnetic method and by image analysis using the SEM. Both methods showed reasonable agreement with each other and similar variations in the progressive reduction in free-iron with increasing additions of ZrB_2

(4) The addition of 1 mole% ZrB_2 significantly reduced the Fe content from 12.34% to 0.84% in the $Nd_{2.2}Fe_{14}B_{1.1}$ BM material.

(5) It was initially observed that the addition of Zr only produced a slight decrease in the formation of Fe, however, this was limited and the Fe content began to increase with increasing Zr.

(6) The addition of 1 mole% TiB_2, ZrB_2 or HfB_2 were all effective in eliminating free-iron from $Nd_2Fe_{14}B$ in BM ingots, suggesting a similar mechanism of a eutectic reaction close to $Nd_2Fe_{14}B$ with the disappearance of the high temperature peritectic reaction at 1 mole% addition of the particular AB_2.

Acknowledgements:

This paper is dedicated to the memory of Dr. Andrew Williams who very sadly passed away during the course of these investigations. The authors would like to thank Less Common Metals Ltd. for their support of this work, including production of book mould alloys and ICP characterisation. Declarations of interest: none

References:

[1] G. Schneider, E.-T. Henig, G. Petzow, H.. Stadelmaier, Phase Relations in the System Fe-Nd-B, Zeitschrift Für Met. 77 (1986) 755–761.

[2] G. Schneider, E.-T. Henig, H.. Stadelmaier, G. Petzow, The Phase Diagram of Fe-Nd-B and the Optimization of the Microstructure of Sintered Magnets, in: 5th Int. Symp.

Magn. Anisotropy Coerc. RE-TM Alloy., Physikalische Blätter, Bad Soden, 1987: pp. 374–362.

[3] J.C. Clarke, I.R. Harris, F.M. Ahmed, Studies of the HDDR Reaction in Stoichiometric Nd-Fe-B Alloys with and without Nb Additions, in: Proc. 14th Int. Work. Rare Earth Perm. Magnets Their Appl., World Scientific, Singapore, Sao Paulo, Brazil, 1996: pp. 482–491.

[4] H. Onodera, Y. Yamaguchi, H. Yamamoto, M. Sagawa, Y. Matsuura, H. Yamamoto, Magnetic properties of a new permanent magnet based on a Nd-Fe-B compound (neomax). I. Mössbauer study, J. Magn. Magn. Mater. (1984). https://doi.org/10.1016/0304-8853(84)90352-4.

[5] B. Hallemans, P. Wollants, J.R. Roos, Thermodynamic Assessment of the Fe-Nd-B Phase Diagram, J. Phase Equilibria. 16 (1995) 137–149.

[6] J. Bernardi, J. Fidler, M. Sagawa, Y. Hirose, Microstructural analysis of strip cast Nd-Fe-B alloys for high (BH)max magnets, J. Appl. Phys. 83 (1998) 6396–6398. https://doi.org/10.1063/1.367557.

[7] S. Ozawa, T. Saito, T. Motegi, Effects of cooling rate on microstructures and magnetic properties of Nd-Fe-B alloys, J. Alloys Compd. 363 (2004) 268–275. https://doi.org/10.1016/S0925-8388(03)00461-4.

[8] R.W. Lee, Hot-pressed neodymium-iron-boron magnets, Appl. Phys. Lett. 46 (1985) 790–791. https://doi.org/10.1063/1.95884.

[9] O. Brooks, A. Walton, W. Zhou, I.R. Harris, The Hydrogen Ductilisation Process (HyDP) for shaping NdFeB magnets, J. Alloys Compd. 703 (2017) 538–547. https://doi.org/10.1016/j.jallcom.2016.12.177.

[10] O.P. Brooks, A. Walton, W. Zhou, D. Brown, I.R. Harris, Complete ductility in NdFeB-type alloys using the Hydrogen Ductilisation Process (HyDP), Acta Mater. 155 (2018). https://doi.org/10.1016/j.actamat.2018.04.055.

[11] V.A. Yartys, O. Gutfleisch, I.R. Harris, Hydrogen-induced phase and magnetic transformations in Nd1.1Fe4B4, J. Magn. Magn. Mater. 157–158 (1996) 119–120. https://doi.org/10.1016/0304-8853(95)01085-8.

[12] D. Brown, A. Williams, O. Gutfleisch, M. Strangwood, I. Harris, Microstructural and Magnetic Studies of Hddr Magnets from High Boron NdFeB(Zr) Alloys, MRS Proc. 577 (1999) 47–55. https://doi.org/10.1557/proc-577-47.

[13] W.G. Moffat, The handbook of binary phase diagrams, Volume 3, General Electric Company, New York, USA, 1978.

[14] T. Tokunaga, K. Terashima, H. Ohtani, M. Hasebe, Thermodynamic Analysis of the Phase Equilibria in the Fe-Zr-B System, Mater. Trans. 49 (2008) 2534–2540. https://doi.org/doi:10.2320/matertrans.MB200809.

[15] H. Okamoto, B-Hf (Boron-Hafnium), Bin. Alloy Phase Diagrams, Second Ed. Ed. T.B. Massalski, ASM Int. Mater. Park. Ohio. 1 (1990) 488–489.

[16] J.L. Murray, P.K. Liao, K.E. Spear, B-Ti (Boron-Titanium), Bin. Alloy Phase Diagrams, Second Ed. Ed. T.B. Massalski, ASM Int. Mater. Park. Ohio. 1 (1990) 544–548.

[17] M. Matzinger, J. Fidler, A. Fujita, I.R. Harris, Micro structure of solid-HDDR Nd-Fe-B:Zr magnets, J. Magn. Magn. Mater. (1996). https://doi.org/10.1016/0304-8853(95)01134-X.

[18] J.C. Clarke, Production and Characterisation of Bonded and Sintered Magnets based on Stoichiometric Nd2Fe14B, University of Birmingham, 1998.

K. Kirby – Investigation, validation, data curation

A. Shaaban – Investigation, validation, data curation

A. Walton – Supervision, project administration, funding acquisition

D. Kennedy – Conceptualization, Resources

A.J.Williams – Conceptualization, Methodology, supervision, project administration, funding acquisition

O.P.Brooks – validation, writing - original draft, writing – review & editing

R.S.Sheridan - writing - original draft, writing – review & editing

I.R.Harris – Conceptualization, Methodology, Resources, writing – original draft, supervision, project administration, funding acquisition